Energetics and Dynamics of Fragmentation of Protonated Leucine Enkephalin from Time- and Energy-Resolved Surface-Induced Dissociation Studies†

Julia Laskin*

Pacific Northwest National Laboratory, Fundamental Science Directorate, P.O. Box 999 (K8-88), Richland, Washington 99352

Received: December 11, 2005; In Final Form: March 9, 2006

Dissociation of singly protonated leucine enkephalin (YGGFL) was studied using surface-induced dissociation (SID) in a Fourier transform ion cyclotron resonance mass spectrometer (FT-ICR MS) specially configured for studying ion activation by collisions with surfaces. The energetics and dynamics of seven primary dissociation channels were deduced from modeling the time- and energy-resolved fragmentation efficiency curves for different fragment ions using an RRKM-based approach developed in our laboratory. The following threshold energies and activation entropies were determined in this study: $E_0 = 1.20$ eV and $\Delta S^{\ddagger} = -20$ eu[1] ($MH^+ \rightarrow \mathbf{b}_5$); $E_0 = 1.14$ eV and $\Delta S^{\ddagger} = -14.7$ eu ($MH^+ \rightarrow \mathbf{b}_4$); $E_0 = 1.42$ eV and $\Delta S^{\ddagger} = -2.5$ eu ($MH^+ \rightarrow \mathbf{b}_3$); $E_0 = 1.30$ eV and $\Delta S^{\ddagger} = -4.1$ eu ($MH^+ \rightarrow \mathbf{a}_4$); $E_0 = 1.37$ eV and $\Delta S^{\ddagger} = -5.2$ eu ($MH^+ \rightarrow$ **y** ions); $E_0 = 1.50$ eV and $\Delta S^{\ddagger} = 1.6$ eu ($MH^+ \rightarrow$ internal fragments); $E_0 = 1.62$ eV and $\Delta S^{\ddagger} = 5.2$ eu ($MH^+ \rightarrow$ F). Comparison with Arrhenius activation energies reported in the literature demonstrated for the first time the reversal of the order of activation energies as compared to threshold energies for dissociation.

Introduction

Fragmentation of peptide ions in the gas phase is central for successful identification of peptides and proteins using tandem mass spectrometry (MS/MS). The resultant MS/MS spectrum is determined by a number of instrumental factors, the internal energy distribution of ions, and by the energetics and mechanisms of dissociation. Studies of fragmentation energetics and mechanisms of gas-phase peptide ions provide the basis for understanding and possibly predicting the MS/MS spectra of biomolecules. However, such studies are challenging because of the size and complexity of the ions. In addition, most of the well-developed experimental approaches that have been successfully employed in the studies of the energetics of fragmentation of small and medium-sized ions are not applicable to the fragmentation of large molecules, for which quantitative approaches are at an early stage of development.

The energetics of fragmentation of large molecules has been extensively studied using blackbody infrared dissociation (BIRD).[1−3] In this method, the ions are heated by radiative exchange with the vacuum chamber walls, and their fragmentation is studied as a function of wall temperature. It has been shown that sufficiently large ions can equilibrate with the blackbody radiation field and have internal energies given by a Boltzmann distribution at a corresponding temperature. Arrhenius parameters for the dissociation of a variety of small ions, peptides, and proteins have been reported.[4−6]

Although BIRD provides a straightforward approach for determination of the activation energy and the pre-exponential factor for dissociation of gas-phase biomolecules, the interpretation of such data is quite complicated because the Arrhenius activation energy contains the contribution associated with reaction entropy. The activation energy, E_a, and the threshold energy, E_0, are connected via the Tolman theorem that can be expressed as follows:[7−10]

$$E_a = E_0 + \langle E^{\ddagger} \rangle - \langle E \rangle + k_B T \tag{1}$$

where k_B is Boltzmann's constant; $\langle E^{\ddagger} \rangle$ and $\langle E \rangle$ are the average energy of the transition state and the average energy of all molecules evaluated at temperature T, respectively. Equation 1 can be rewritten in the following form:

$$E_a = E_0 + \Delta E_{corr} + k_B T \tag{2a}$$

where ΔE_{corr} is Tolman's correction factor given by

$$\Delta E_{corr} = k_B T^2 \frac{\partial \ln Q^{\ddagger}/Q}{\partial T} \tag{2b}$$

and $Q^{\ddagger}$ and Q are partition functions of the transition state and the excited molecule, respectively. The entropy of activation is given by eq 3:

$$\Delta S^{\ddagger} = k_B \ln \frac{Q^{\ddagger}}{Q} + k_B T \frac{\partial \ln Q^{\ddagger}/Q}{\partial T} \tag{3}$$

Clearly, Tolman's correction factor (eq 2b), hence the activation energy (eq 2a), is correlated with the activation entropy through the second term in eq 3. As a result, Arrhenius activation energies are strongly correlated with pre-exponential factors (A) and do not necessarily reflect the relative stability of ions toward dissociation.[11] For example, for reactions proceeding via a very tight transition state (TS) (low pre-exponential factors), ΔE_{corr} is negative and the Arrhenius activation energy is lower than the threshold energy, while for reactions characterized by a loose TS (high pre-exponential factor) the Arrhenius activation energy is higher than the threshold energy for reaction. We have demonstrated that Tolman's correction factor increases almost

† Part of the "Chava Lifshitz Memorial Issue".

* Corresponding author. Tel.: (509) 376-4443. Fax: (509) 376-6066. E-mail: julia.laskin@pnl.gov.

10.1021/jp057229r CCC: $33.50
Published on Web 04/11/2006

linearly with Log(A) and ranges from −14 kcal/mol for Log(A) of 6 to 36.4 kcal/mol for Log(A) of 39.2.[11]

This analysis suggests that the strong correlation between the Arrhenius parameters can reverse the order of Arrhenius activation energies for different systems relative to the order of the corresponding threshold energies. Converting E_a into the threshold energy, E_0, using Tolman's theorem reveals the true magnitude of the correlation between molecular complexity and stability. In this study, we will demonstrate the reversal of the order of activation energies for the two major dissociation pathways of protonated leucine enkephalin. Threshold energies and reaction entropies will be derived using an RRKM-based modeling of the time- and energy-resolved surface-induced dissociation (SID) data described by us previously.[12,13] Thermal dissociation rates and the corresponding Arrhenius parameters will be deduced by averaging the calculated microcanonical rate constants over thermal distributions at different temperatures.

Dissociation of protonated leucine enkephalin (YGGFL) in the gas phase has been extensively studied using a variety of experimental approaches.[14−23] Both BIRD and ion trap collision-induced dissociation (CID) experiments were utilized to study thermal kinetics of dissociation of YGGFL.[24,25] A relatively simple dissociation pattern and well-established thermal kinetics make YGGFL an excellent "thermometer" ion for characterization of internal energy deposition into peptide ions in different ionization and activation processes.[26−28]

Here, we present a detailed study of the SID of protonated leucine enkephalin on a self-assembled monolayer surface (SAM). This ion activation method originally introduced by Cooks and co-workers[29,30] has been extensively reviewed.[31−33] It provides an efficient means for very fast, single-step excitation of the ion in which internal energy deposition occurs in a few picoseconds.[34] We have demonstrated that this single-step ion activation combined with the long and variable time scale of a Fourier transform ion cyclotron resonance mass spectrometer (FT-ICR MS) is perfectly suited for studying the energetics and dynamics of peptide fragmentation.[35,36] The advantages provided by SID include very fast ion activation, which eliminates possible discrimination against higher-energy dissociation pathways,[37] and efficient "amplification" of small changes in dissociation parameters.[38] The large kinetic shift, the internal energy in excess of the threshold energy required to produce detectable dissociation of a polyatomic ion on the time scale of a mass spectrometer, and the partial (typically 10−20%) transfer of the kinetic to internal energy in ion-surface collision are the two major effects that contribute to the amplification, which makes SID a very sensitive probe of the fragmentation energetics and dynamics.

Experimental Section

Surface-induced dissociation experiments were conducted on a specially fabricated 6T FT-ICR mass spectrometer.[39] The instrument is equipped with a high-transmission electrospray source, consisting of an ion funnel interface[40] followed by three quadrupoles that provide for pressure drop and ion bunching, mass selection, and ion accumulation, respectively. The SID target is introduced through a vacuum interlock assembly and is positioned at the rear trapping plate of the ICR cell. Both the instrument and the SID experimental protocol have been detailed elsewhere[39] and will be only briefly outlined below.

Ions are electrosprayed, at atmospheric pressure, into the end of a heated stainless steel capillary tube. The ion funnel that follows the capillary provides highly efficient ion transfer into the high vacuum region of the mass spectrometer. Three quadrupoles following the ion funnel provide collisional focusing, mass selection of the ion of interest, and accumulation of ions external to the ICR cell. Typical accumulation times used in this study were in the range of 0.1−0.3 s. The third (accumulation) quadrupole is held at elevated pressure (about 2×10^{-3} Torr) for collisional relaxation of any internal energy possessed by ions generated by electrospray ionization prior to their injection into the ICR cell.

After accumulation, ions are extracted from the third quadrupole and transferred into the ICR cell where they collide with the surface. Scattered ions are captured by raising the potentials on the front and rear trapping plates of the ICR cell by 10−20 V. Time-resolved mass spectra were acquired by varying the delay between the gated trapping and the excitation/detection event (the reaction delay). The reaction delay was varied from 1 ms to 1 s. Immediately following the fragmentation delay, ions were excited by a broadband chirp and detected. The collision energy is defined by the difference in the potential applied to the accumulation quadrupole and the potential applied to the rear trapping plate and the SID target. The ICR cell can be offset above or below ground by as much as ±150 V. Lowering the ICR cell below ground while keeping the potential on the third quadrupole fixed increases collision energy for positive ions.

Experimental control is accomplished with a MIDAS data station developed by Marshall and co-workers at the National High Magnetic Field Laboratory.[41] MIDAS is used to control the voltages and timing of the ion source and transfer optics, as well as ion manipulation in the ICR cell. An automated script was written to allow for unattended acquisition of the kinetic data. The script was used to vary the fragmentation delay and collision energy of the experiment. Reaction delays of 1 ms, 5 ms, 10 ms, 50 ms, 0.1 s, and 1 s were studied. Typical experiments involved changing the collision energy across a relatively wide range from 7 to 55 eV in 2 eV increments at each of the six reaction delays. Time-dependent fragmentation efficiency curves (TFECs) were constructed from experimental mass spectra by plotting the relative abundance of the precursor ion and its fragments as a function of collision energy for each delay time.

The SAM surface was prepared on a single gold {111} crystal (Monocrystals, Richmond Heights, OH) using a standard procedure. The target was cleaned in a UV cleaner (model 135500, Boekel Industries Inc., Feasterville, PA) for 10 min and allowed to stand in a 98% 1-dodecanethiol thiol ($CH_3(CH_2)_{11}$-SH) solution (Sigma-Aldrich) for 8−12 h. The target was removed from the SAM solution and ultrasonically washed in ethanol for 10 min to remove extra layers.

Leucine enkephalin was purchased from Sigma and used as received. The sample was dissolved in a 50:50 (v/v) methanol: water solution with 1% acetic acid to a final concentration of 20−50 μM. A syringe pump (Cole Parmer, Vernon Hills, IL) was used for direct infusion of the electrospray samples at 20 μL/h.

RRKM Modeling. TFECs were modeled using an RRKM-based approach developed by our group.[12,13] Microcanonical rate constants as a function of internal energy for all reaction channels were calculated using the RRKM/QET expression.[8,42] The breakdown graph (BDG), a collection of breakdown curves (BDC) representing fragmentation probability of the precursor ion into a particular reaction channel as a function of the internal energy of the precursor ion (E) and the reaction time (t_r), is calculated using the appropriate equations of formal kinetics derived for a particular reaction scheme. Because of the long

reaction delay times involved in our FT-ICR SID experiments, radiative cooling of excited ions must be taken into account. The same radiative rate, k_{rad}, is used to model radiative cooling of the precursor ion and its fragments.

The energy deposition function is described by the following analytical expression:[12,13]

$$P(E,E_{coll}) = (E - \Delta)^l \exp(-(E - \Delta)/f(E_{coll}))/C \quad (4)$$

where l and Δ are parameters, $C = \Gamma(l + 1)[f(E_{coll})]^{l+1}$ is a normalization factor, and $f(E_{coll})$ has the form:

$$f(E_{coll}) = A_2 {E_{coll}}^2 + A_1 E_{coll} + E_{th}/(l + 1) \quad (5)$$

where A_1 and A_2 are parameters, E_{th} is the thermal energy of the ensemble of peptide ions prior to ion activation, and E_{coll} is the collision energy. Finally, the normalized signal intensity for a particular reaction channel is given by the equation:

$$I_i(E_{coll}) = \int_0^\infty \mathrm{BDC}_i(E,t_r) P(E,E_{coll})\, \mathrm{d}E \quad (6)$$

Calculated TFECs were constructed using the above procedure and compared to experimental data. The energy deposition function was kept the same for all reaction times. The fitting parameters were varied until the best fit to experimental curves was obtained. The fitting parameters included the critical energy and the activation entropy for all reaction channels and the parameters characterizing the energy deposition function (eqs 4,5). The uniqueness of the fits was confirmed using the sensitivity analysis described previously.[13] Specifically, the critical energy of reaction 2 ($MH^+ \rightarrow \mathbf{b}_4$) was systematically changed in increments of 0.02 eV, and the rest of the fitting parameters were adjusted to give the best fit. This test revealed that dissociation energies for all primary dissociation channels and most of the secondary reactions are unique within 0.05 eV; a larger uncertainty of 0.15 eV was obtained for reaction 10. Although the model utilizes a large number of fitting parameters, fitting time- and energy-dependent branching ratios of different dissociation pathways imposes serious constraints on fitting parameters. Energy dependence of branching ratios is largely determined by the relative values of activation entropies. As a result, activation entropies remained unchanged during the sensitivity analysis described here. It has been also confirmed that the data could not be reproduced reasonably well using different values of activation entropies.

Vibrational frequencies of the precursor ion were obtained from the frequency model given by Christie.[43] Vibrational frequencies for the transition state were estimated by removing one C−N stretch (reaction coordinate) from the parent ion frequencies as well as varying all frequencies in the range of 500−1000 cm^{-1} to obtain the best fit with experimental data.

Energy Partitioning. Energy partitioning between ionic and neutral fragments must be taken into account for accurate modeling of consecutive dissociation pathways. In general, the internal energy of an ionic fragment formed from a precursor ion with internal energy, E, does not exceed $E - E_0$ (where E_0 is the critical energy for the reaction) and equals $E - E_0$ only when a neutral fragment cannot carry away any internal energy, that is, for monatomic neutral fragments. The fraction of the internal energy carried off by the neutral increases with increasing complexity of the neutral fragment. In our study of the fragmentation of bromonaphthalene radical cation, we have shown that partitioning of energy between the ionic and neutral products must be included in the modeling of the fragmentation kinetics of complex systems.[13] This can be done (assuming that the excess energy is partitioned statistically among the fragments) by calculating all permutations of the energy partitioning from densities of states of the ionic and neutral fragments. Given the total internal energy in the precursor ion (E), the probability that the internal energy of the ionic fragment is between ϵ and $\epsilon + \mathrm{d}\epsilon$ is given by:[44,45]

$$p(E,\epsilon) = \frac{\rho_1(\epsilon)\rho_2(E - E_0 - \epsilon)\, \mathrm{d}\epsilon}{\int_0^{E - E_0} \rho_1(\epsilon)\rho_2(E - E_0 - \epsilon)\, \mathrm{d}\epsilon} \quad (7)$$

where ρ_1 and ρ_2 are the densities of states of ionic and neutral fragments, respectively.

Equation 7 is used to calculate the internal energy distribution of ionic fragments for each internal energy, E, of the precursor ion. The most probable internal energy retained by the ionic fragment, E_{mp}, is obtained from the maximum of the distribution. In our modeling procedure, the dependences of E_{mp} on $E - E_0$ for each reaction are fitted with a second-order polynomial, and the analytical functional form obtained in this way is used to calculate the internal energy content of different fragment ions.

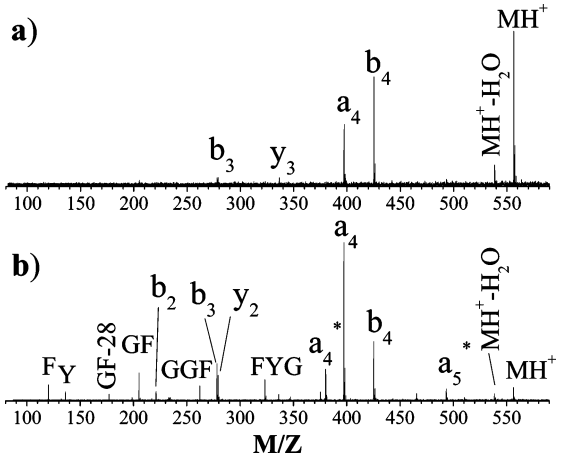

Figure 1. 30 eV (a) and 50 eV (b) SID spectra of protonated leucine enkephalin obtained using the HSAM surface as a target and reaction delay of 1 s.

Results

In this study, we examined SID of singly protonated leucine enkephalin (YGGFL) colliding with a SAM of 1-dodecane thiol on gold (HSAM). We have previously demonstrated that the energy transfer efficiency on HSAM surfaces is relatively small and fragmentation occurs at high collision energies, thereby minimizing ion loss on the surface. A proper choice of the SID target is very important for protonated leucine enkephalin as a projectile ion. Our initial studies showed that YGGFL fragments at less than 10 eV collision energy when the fluorinated SAM (FSAM) surface is used as a target. In this energy regime, soft landing or neutralization on the surface is the dominant process and the intensity of scattered ions is quite low.[46,47] However, because of the lower-energy transfer efficiency, SID of leucine enkephalin by collisions with the HSAM surface occurs at significantly higher collision energies than on the FSAM surface; this helps to substantially reduce ion loss and improve the signal-to-noise ratio in SID spectra.

Figure 1 shows representative SID spectra of YGGFL for 30 and 50 eV collisions with the HSAM surface and reaction delay of 1 s. SID spectra shown in Figure 1 are similar to MS/MS spectra of leucine enkephalin reported in the literature.[14−26] At low collision energies, fragmentation is dominated by the

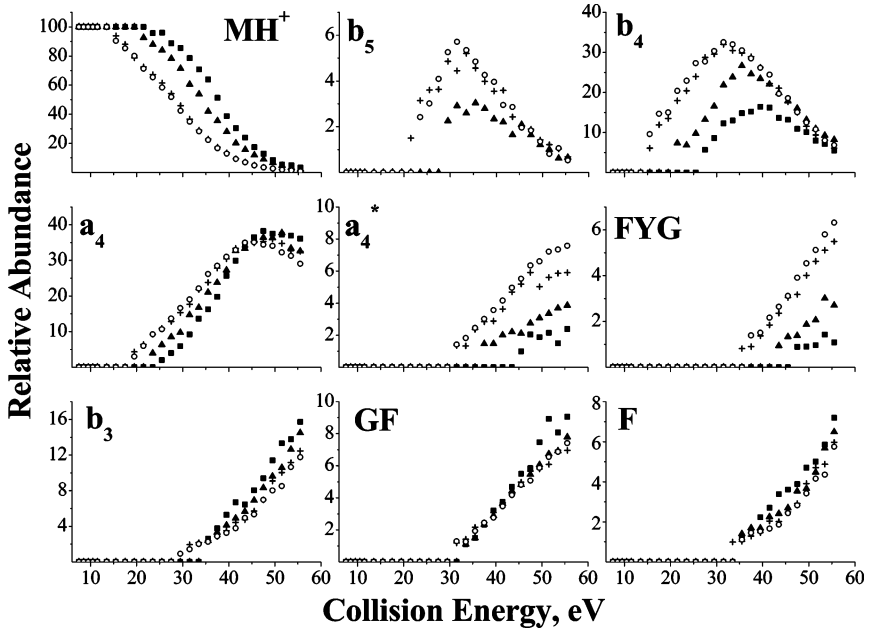

Figure 2. Time- and energy-dependent fragmentation efficiency curves (TFECs) for the protonated YGGFL and its major fragments at reaction delays of 1 ms (■), 5 ms (▲), 50 ms (+), and 1 s (○).

formation of the $\mathbf{b}_4/\mathbf{a}_4$ ion pair and loss of water from the protonated precursor ion resulting in formation of the $\mathbf{b}_5$ ion. SID spectrum obtained at 50 eV collision energy contains a large number of sequence specific fragments including an almost complete series of $\mathbf{b}_n$ ions ($\mathbf{b}_2-\mathbf{b}_5$) and $\mathbf{y}_n$ ions ($\mathbf{y}_1-\mathbf{y}_3$), a number of $\mathbf{a}_n$ and $\mathbf{a}_n$-NH_3 ions ($\mathbf{a}_5$, $\mathbf{a}_5$*, $\mathbf{a}_4$, $\mathbf{a}_4$*), a series of internal fragments (GGF, GGF−CO, GF, GF−CO), and immonium ions (F, Y). The formation of a rearrangement fragment labeled FYG (*m*/*z* 323) in Figure 1b has been discussed in detail by Glish and co-workers.[21] They demonstrated that the formation of this ion involves the loss of an internal glycine residue (*m*/*z* 57) and NH_3 from the $\mathbf{a}_4$ ion.

Different fragment ions of YGGFL exhibit very different kinetic behavior. Figure 2 shows time- and energy-dependent fragmentation efficiency curves (TFECs) for the parent ion and eight most abundant fragments at four reaction delays. Strong time dependence is observed for the precursor ion and several fragments including $\mathbf{b}_5$, $\mathbf{b}_4$, $\mathbf{a}_4$*, and FYG. TFECs of the $\mathbf{a}_4$ ion show significantly weaker time dependence, while TFECs of the $\mathbf{b}_3$, GF, and F fragments do not display any time dependence on the time scale examined in our experiments. It can be concluded that the formation of the $\mathbf{b}_5$, $\mathbf{b}_4$, $\mathbf{a}_4$*, and FYG ions is associated with substantial rearrangements, while the formation of the $\mathbf{a}_4$, $\mathbf{b}_3$, GF, and F ions follows entropically favored pathways. The observed kinetic behavior of different fragment ions shown in Figure 2 will be used for critical analysis of the possible dissociation pathways for YGGFL in our FT-ICR SID experiments.

Dissociation Pathways. Detailed modeling of dissociation of protonated leucine enkephalin and the energetics and kinetics of formation of its fragments requires knowledge of dissociation pathways following ion activation. Dissociation pathways of protonated leucine enkephalin have been extensively studied using a variety of ion activation techniques including high-energy single-collision activation,[19] low-energy multiple-collision CID,[14,16,21−23] and blackbody infrared irradiation.[24]

The first systematic study describing dissociation pathways of YGGFL was reported by Alexander and Boyd.[14] They summarized low-energy (5−120 eV in the laboratory frame) CID routes for MH^+ in an rf-only quadrupole as shown in

SCHEME 1

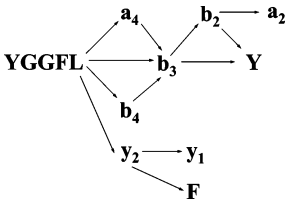

Scheme 1. According to this study, the $\mathbf{b}_4$, $\mathbf{a}_4$, $\mathbf{b}_3$, and $\mathbf{y}_2$ ions are formed directly from the parent ion, while the $\mathbf{b}_2$ and $\mathbf{y}_1$ ions result from consecutive dissociation of the primary fragments. Further fragmentation of the N-terminal fragments results in formation of the tyrosine immonium ion (Y), while phenylalanine immonium ion (F) is produced from the $\mathbf{y}_2$ ion.

A significantly more complicated dissociation scheme was proposed by Ballard and Gaskell from the analysis of metastable and collision-induced dissociation of YGGFL.[16] They suggested that the reaction sequence $MH^+ \rightarrow \mathbf{b}_4 \rightarrow \mathbf{a}_4$ plays an important role in the formation of the $\mathbf{a}_4$ ion, although it can be also formed via the $MH^+ \rightarrow \mathbf{a}_4$ pathway. Second generation product spectra reported in this study suggest that $\mathbf{y}_1$ and $\mathbf{y}_2$ and F ions are produced from the $\mathbf{y}_3$ and $\mathbf{y}_4$ fragments. The $\mathbf{a}_4$ ion is a precursor for the $\mathbf{b}_3$, $\mathbf{b}_2$, a_2, F, and Y fragment ions. The GF and GF−CO ions are mainly formed from the $\mathbf{y}_3$ ion, although at long reaction times these fragments can also originate from the $\mathbf{a}_4$ ion; $\mathbf{b}_4$, $\mathbf{y}_4$, and $\mathbf{y}_4$-$\mathbf{H_2O}$ were all detected as precursors of the GGF fragment, while GGF−CO is most likely formed from the $\mathbf{y}_4$ and $\mathbf{a}_4$ ions.

Although similar dissociation patterns have been observed for YGGFL in different instruments, the partitioning between various fragmentation pathways has a notable dependence on the ion activation method. For example, while the experiments utilizing relatively fast excitation in hybrid sector/rf quadrupole instruments showed that a large fraction of the $\mathbf{a}_4$ ions is formed directly from the MH^+ ion, double resonance CID experiments in an ion trap suggested that only 11% of all $\mathbf{a}_4$ ions are formed from the parent ion and 87% from the $\mathbf{b}_4$ ion.[22] Williams and co-workers found that in BIRD experiments the $\mathbf{a}_4$ ion is formed exclusively from the $\mathbf{b}_4$ ion.[24] Similarly, low-amplitude multiple-

SCHEME 2

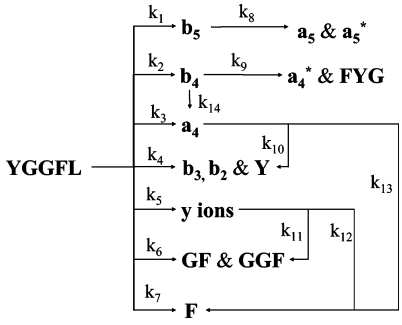

resonance CID in a collision cell reported by Rakov et al. showed that in these experiments all N-terminal fragments are formed by consecutive dissociation of the $\mathbf{b}_4$ ion, while the internal GF and GGF fragments are produced primarily from the $\mathbf{y}_3$ and $\mathbf{y}_4$ ions.[23] These results suggest that the consecutive $MH^+ \rightarrow \mathbf{b}_4 \rightarrow \mathbf{a}_4$ pathway plays an important role when the precursor ion is excited very slowly, while fast excitation of the precursor ion favors the formation of the $\mathbf{a}_4$ ion directly from the MH^+ ion.

Because ion-surface collisions result in very fast ion activation, we used an expanded version of Scheme 1 in our modeling of time- and energy-resolved SID data. The dissociation scheme that provided the best description of our SID data is shown in Scheme 2, in which dissociation of YGGFL is described using seven primary and seven secondary reactions. The reaction scheme was simplified by combining several fragments together and modeling their cumulative abundance. For example, reaction 6 describes the formation of GF, GF−CO, GGF, and GGF−CO fragments. Formation of the $\mathbf{b}_3$, $\mathbf{b}_2$, and Y ions is described using a single rate constant, k_4. This is a reasonable approach because according to Scheme 1 the $\mathbf{b}_2$ and Y ions are formed by consecutive fragmentation of the $\mathbf{b}_3$ ion. Reaction 5 describes the cumulative formation of $\mathbf{y}_1$, $\mathbf{y}_2$, and $\mathbf{y}_3$ ions from the precursor ion. The most abundant ions in this family of fragments are the $\mathbf{y}_2$ and $\mathbf{y}_3$ ions that account for ca. 70% and 30% of the relative abundance of **y** ions, respectively. As a result, dissociation parameters for reaction 5 mainly reflect the energetics and dynamics of formation of the $\mathbf{y}_2$ ion from the protonated peptide. Similar kinetics and strong time dependence observed for the $\mathbf{a}_4$* and FYG ions suggest that they are likely produced from the $\mathbf{b}_4$ ion. Finally, the products of the $\mathbf{b}_5$ ion ($\mathbf{a}_5$ and $\mathbf{a}_5$*) were combined together, and their formation was described using a single rate constant, k_8.

Scheme 2 assumes that the total decomposition of the protonated precursor ion is determined by seven primary dissociation channels as compared to four primary channels proposed by Alexander and Boyd (Scheme 1).[14] Clearly, the $\mathbf{b}_5$ ion not included in Scheme 1 is formed by loss of a water molecule from the protonated YGGFL. Our initial attempts to model the formation of GGF ions and phenylalanine immonium ion via consecutive pathways did not give a satisfactory agreement between the experimental and calculated TFECs for these fragments. Reactions 6 and 7 were added to the dissociation scheme for adequate description of the time and energy dependence of the formation of these fragment ions.

Secondary reactions in Scheme 1 include the well-established consecutive $\mathbf{b}_4 \rightarrow \mathbf{a}_4$ and $\mathbf{b}_5 \rightarrow \mathbf{a}_5$ pathways, subsequent fragmentation of the $\mathbf{a}_4$ and **y** ions into the phenylalanine immonium ion (F), and the formation of $\mathbf{b}_3$, $\mathbf{b}_2$, and Y ions from the $\mathbf{a}_4$ ion. The latter channel suggested by Ballard and Gaskell was discussed earlier.[16] Although all seven secondary reaction channels were incorporated into the modeling, we found that the rate constants for reactions 12−14 obtained from the best fit of the experimental data were too slow and these reactions could not compete with the alternative primary dissociation channels. It follows that according to our modeling the $\mathbf{b}_4 \rightarrow \mathbf{a}_4$ reaction that plays a very important role in slow ion activation experiments does not contribute significantly to the formation of the $\mathbf{a}_4$ ion in SID experiments, in which internal excitation of the precursor ion occurs on a picosecond time scale.

RRKM Modeling. TFECs of different fragments were modeled using an approach described earlier. The breakdown graph was calculated using the appropriate equations of formal kinetics derived for Scheme 2. The parameters of the energy deposition function and dissociation parameters (critical energies and activation entropies) characterizing the rate-energy dependence of the 14 dissociation rate constants shown in Scheme 2 were varied to obtain the best fit of experimental TFECs at six different reaction delays.

Figure 3 shows the comparison between the experimental data at four reaction delays and best fits obtained from the modeling. Despite the complexity of the model and a number of simplifying assumptions involved in constructing the reaction scheme, the agreement between the experiment and the model is fairly good. Dissociation parameters for the seven primary reactions 1−7 obtained from the best fit are listed in Table 1, and the microcanonical rate-energy dependences are shown in Figure 4. Because of the simplifying assumptions used to establish parent−fragment relationships described earlier, the parameters obtained for the secondary dissociation pathways are characterized by large uncertainties and will not be discussed here.

Discussion

Rate Constants and Dissociation Parameters. The results summarized in Table 1 indicate that the lowest-energy channels for the fragmentation of protonated leucine enkephalin correspond to the formation of $\mathbf{b}_4$ and $\mathbf{b}_5$ ions. The lowest-energy channels are characterized by the largest negative activation entropies, suggesting that structural rearrangements occur during the formation of these fragment ions. This finding is in agreement with our previous studies, in which we showed that low-energy dissociation pathways of protonated peptides are commonly associated with fairly tight transition states.[36,48] Formation of the $\mathbf{b}_4$ ion is both energetically and entropically more favorable than the loss of water molecule from the precursor ion resulting in formation of the $\mathbf{b}_5$ ion, consistent with our previous studies of the energetics of fragmentation of small alanine-containing peptides.[35,49]

Formation of an abundant $\mathbf{b}_4$ ion is in agreement with the general tendency of nonbasic peptides to yield abundant $\mathbf{b}_{n-1}$ fragment ions. Our modeling suggests that the formation of the $\mathbf{b}_4$ ion of YGGFL is 0.28 eV (6.5 kcal/mol) more favorable than the formation of a smaller $\mathbf{b}_3$ ion via reaction 4.[50] It is interesting to compare this result to the relative energetics of formation of $\mathbf{b}_4$ and $\mathbf{b}_3$ ions of another nonbasic pentapeptide, AAAAA, obtained by Paizs and Suhai using DFT calculations.[51] This study showed that the $MH^+ \rightarrow \mathbf{b}_4$ pathway for protonated pentaalanine is ca. 8−9 kcal/mol more favorable than the $MH^+ \rightarrow \mathbf{b}_3$ pathway. Our results are in good qualitative agreement with this computational study.

The energetics of formation of the $\mathbf{b}_3/\mathbf{y}_2$ ion pair via reactions 4 and 5 is also consistent with the behavior reported for pentaalanine. Dissociation parameters and rate-energy dependences for these two reactions are very similar. Paizs and Suhai suggested that these complementary ions are formed via the

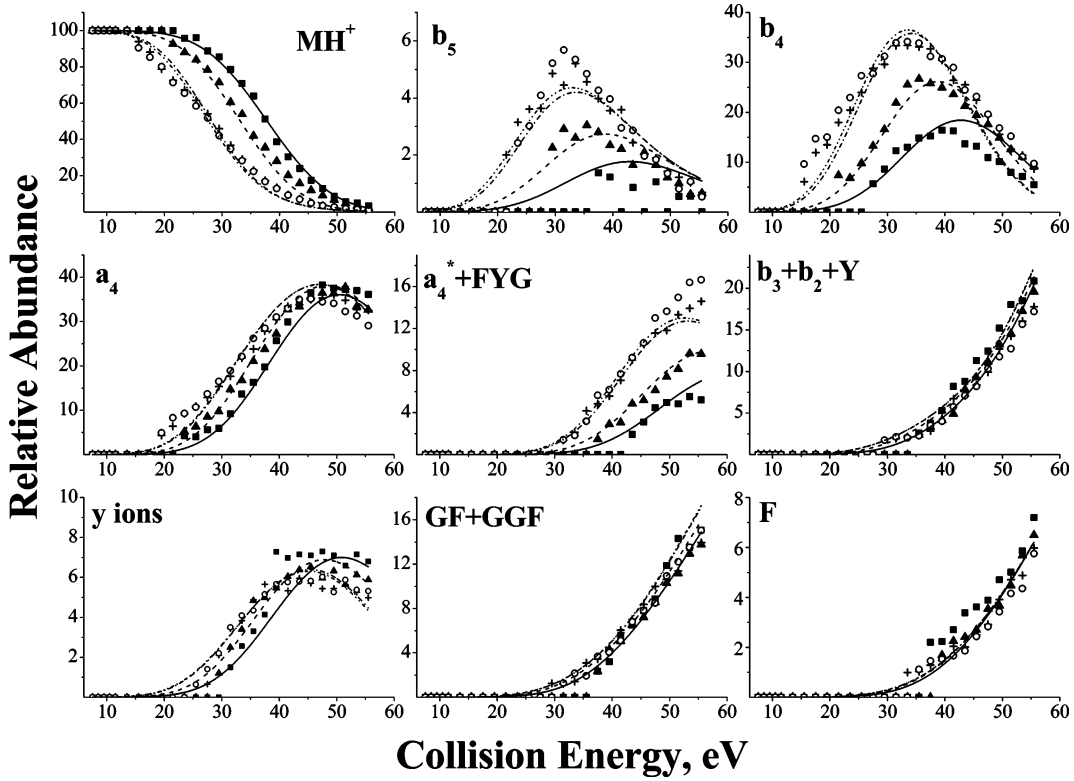

Figure 3. RRKM modeling fit of experimental data for dissociation of YGGFL. Experimental and calculated TFECs correspond to reaction delays of 1 ms (■, solid lines), 5 ms (▲, dashed lines), 50 ms (+, dash−dot lines), and 1 s (○, dash−dot−dot lines).

TABLE 1: Results of the RRKM Modeling of the TFECs of Primary Fragmentation Channels of YGGFL

	fragment						
	$\mathbf{b}_5$	$\mathbf{b}_4$	$\mathbf{a}_4$	$\mathbf{b}_3$ and $\mathbf{b}_2$ and Y	**y** ions	GF and GGF	F
	k_1	k_2	k_3	k_4	k_5	k_6	k_7
E_0, eV	1.20	1.14	1.30	1.42	1.37	1.50	1.62
$\Delta S^{\ddagger}$, eu	−20.0	−14.7	−4.1	−2.5	−5.2	1.6	5.2
A, s^{-1}	1.1×10^9	1.5×10^{10}	3.3×10^{12}	7.4×10^{12}	1.9×10^{12}	5.8×10^{13}	3.5×10^{14}
E ($k = 1$ s^{-1}), eV	3.38	2.94	3.42	3.90	3.78	4.06	4.38

same proton-bound intermediate complex and their relative abundance in MS/MS spectra is determined only by relative proton affinities of the corresponding neutral molecules.[51] They described the formation of such fragment ion pair using a single rate constant. Our results indicate that there is a small but measurable difference in both energy and entropy effects of the two reactions: $MH^+ \rightarrow \mathbf{b}_3$ and $MH^+ \rightarrow \mathbf{y}_2$. In particular, the reaction resulting in the formation of the $\mathbf{y}_2$ ion has somewhat lower threshold energy and more negative activation entropy, suggesting that the formation of this ion requires more significant rearrangement than the formation of the corresponding $\mathbf{b}_3$ ion.

The highest-energy primary reaction channels of YGGFL, reactions 6 and 7, correspond to the formation of GF and GGF internal fragments and the phenylalanine immonium ion (F). Cleavage of two amide bonds is required for the formation of these fragments, one of which is the fourth amide bond between the phenylalanine and the leucine residues. Interestingly, the same bond cleavage results in formation of the most abundant $\mathbf{b}_4$ and $\mathbf{a}_4$ ions, suggesting that this is the most labile bond in protonated leucine enkephalin. Cumulatively, cleavage of this bond accounts for more than 60% fragmentation of YGGFL. Analysis of site-specific H/D exchange rates performed by Lifshitz and co-workers suggested that YGGFL is protonated at the N-terminal amino group.[52] Preferential cleavage of the fourth peptide bond requires a transfer of the ionizing proton from the N-terminus to another side of the peptide. This can be explained only based on the secondary structure of the peptide. Interestingly, DFT calculations of the structure of the neutral form of leucine enkephalin[53] demonstrated the formation of a bifurcated hydrogen bond between the oxygen of the fourth carbonyl group, the N-terminal amino group, and the hydrogen of OH group of the C-terminal COOH group. It follows that even in a neutral form the fourth carbonyl group of YGGFL is strongly bound to the N-terminus. In the neutral molecule, this binding is facilitated by the C-terminal acidic hydrogen, while in the protonated ion this hydrogen bond is most likely facilitated by the ionizing proton. It is expected that hydrogen bonding between the fourth carbonyl group of YGGFL and the N-terminal amino group is even stronger in the presence of the ionizing proton at the N-terminus. From the above discussion, it follows that secondary structure of the protonated leucine enkephalin is responsible for the preferential formation of the $\mathbf{b}_4$, $\mathbf{a}_4$, GGF, GF, and F fragments.

Facile formation of the $\mathbf{a}_4$ ion directly from the protonated parent ion is a rather unexpected result; reaction 3 is the third lowest-energy reaction channel of YGGFL. Earlier discussion also showed that in our SID experiments the alternative consecutive pathway involving loss of CO from the $\mathbf{b}_4$ ion cannot compete with the $MH^+ \rightarrow \mathbf{a}_4$ pathway. Reaction 3 has a higher threshold energy and more positive entropy effect than reactions 1 and 2, which allows this reaction to efficiently

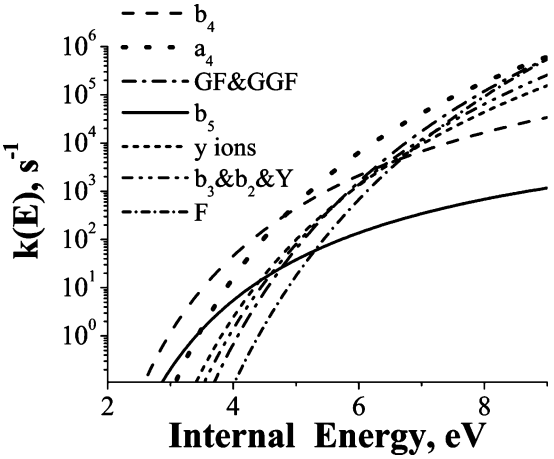

Figure 4. Microcanonical rate-energy dependences for the primary fragmentation pathways of protonated YGGFL.

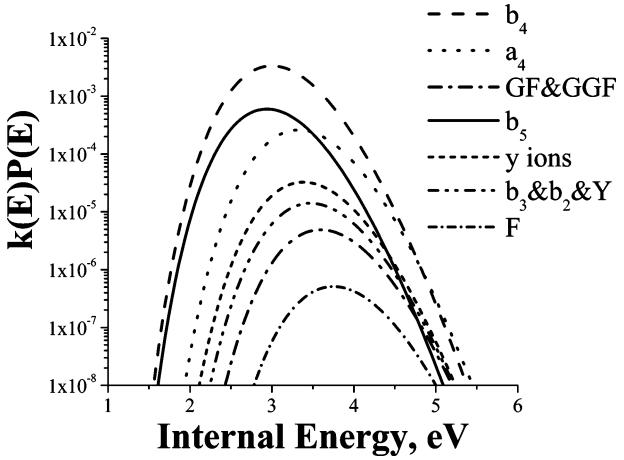

Figure 5. Reactive populations, $k(E)P(E)$, calculated using rate-energy dependences shown in Figure 4 and the thermal distribution, $P(E)$, at 450 K.

compete with lower-energy pathways even at low internal energies. However, this and other higher-energy dissociation pathways of YGGFL will be strongly suppressed in slow heating experiments.[54] We have demonstrated that multiple-collision CID, a slow activation method, strongly discriminates against fragment ions formed via competitive high-energy reaction channels.[37] When the lowest-energy channel opens up, dissociation efficiency through the higher-energy channel is determined by the rate of ion activation. If activation is slow as compared to dissociation through the low-energy pathway, the fragment corresponding to the higher-energy pathway is strongly suppressed. As a result, contribution of reactions 3−7 to the formation of fragment ions in MS/MS experiments is a strong function of the rate of ion activation.

In our previous study, we modeled the total decomposition of the protonated leucine enkephalin using a single rate constant. Dissociation parameters obtained from such modeling were $E_0 = 1.13$, $\mathrm{Log}(A) = 11.4$.[55] The total decomposition rate of YGGFL determined by combining individual decay rates of primary reaction channels shown in Figure 4 is best described using $E_0 = 1.13$, $\mathrm{Log}(A) = 10.9$. It follows that modeling presented in this study is in excellent agreement with our previously published model of the total decomposition of leucine enkephalin. It is also consistent with SID results obtained in a double quadrupole instrument, in which fragmentation occurs on a microsecond time scale.[31] Wysocki and co-workers estimated that the most probable internal energy of YGGFL ions fragmenting in a double quadrupole instrument is 8 eV.[56] The total decomposition rate at 8 eV internal excitation determined from our modeling is $5 \times 10^5\ \mathrm{s}^{-1}$ corresponding to the lifetime of 2 μs.

Comparison with Thermal Kinetics. Thermal kinetics of YGGFL has been studied using BIRD[24] and rf heating in an ion trap.[26] Both studies suggest that in thermal experiments the $\mathbf{b}_4$ and $\mathbf{b}_5$ are the only primary fragment ions. Reactive populations of different primary fragments were calculated for comparison with thermal kinetics experiments. The reactive population is given by the product of the microcanonical rate constant $k(E)$ and a Boltzmann distribution of internal energies, $P(E)$, at a particular temperature. Figure 5 shows reactive populations calculated using $k(E)$ curves shown in Figure 4 and the thermal distribution at the average temperature of BIRD experiments, 450 K. The calculated branching ratio between reactions 1 and 2 is 0.17. This result is in excellent agreement with the value of 0.18 at 429 K and 0.132 at 476 K reported by Williams and co-workers.[24] From the calculated reactive population, it is estimated that only less than 8% of $\mathbf{a}_4$ ions are formed directly from the precursor ion in thermal experiments, while all other higher-energy dissociation pathways cumulatively contribute less than 1.5% to the total decomposition of the precursor ion.

The Arrhenius parameters for the total decomposition of YGGFL determined from BIRD experiments are $E_a = 1.09$ eV and $\mathrm{Log}(A) = 10.5$.[24] The dissociation threshold derived from the Arrhenius activation energy is 1.18 eV.[57] The low pre-exponential factor indicates a tight transition state. The pre-exponential factor derived from our modeling (Table 1) is $10^{10.2}$, in excellent agreement with BIRD data. The following Arrhenius activation parameters were reported for reactions 1 and 2: $E_a(1) = 0.99$ eV, $\mathrm{Log}(A_1) = 8.7$ and $E_a(2) = 1.11$ eV, $\mathrm{Log}(A_2) = 10.7$.[24] From the modeling of SID data, we derived the following values of threshold energies and pre-exponential factors at 450 K: $E_0(1) = 1.20$ eV, $\mathrm{Log}(A_1) = 9.0$ and $E_0(2) = 1.14$ eV, $\mathrm{Log}(A_2) = 10.2$. Despite a very good correspondence between the pre-exponential factors determined using these absolutely different approaches, there is a clear disagreement between Arrhenius activation energies and threshold energies derived from our modeling. Specifically, while thermal experiments suggest that reaction 1 has a lower threshold than reaction 2, threshold energies follow an opposite trend.

This discrepancy is readily rationalized using Tolman's theorem analysis discussed in the Introduction. Threshold energy for reaction representing the stability of the ion toward fragmentation is related to the Arrhenius activation energy through eq 2a. In our previous studies, we suggested that correlation between the Arrhenius activation parameters is significant and can alter the order of activation energies as compared to the corresponding threshold energies. This is exactly the reason for the difference between the energetics of reactions 1 and 2 reported in this study and the Arrhenius energies determined in BIRD experiments.

To illustrate this point, we used dissociation parameters obtained in this study to calculate Tolman's correction factors and Arrhenius activation energies for reactions 1 and 2 at different temperatures using eqs 2a and 2b, respectively. The results are plotted in Figure 6. At low temperatures, Arrhenius activation energies are closely approximated by the corresponding threshold energies. With increase in temperature, the values of Arrhenius energies decrease. The rate of this decrease is determined by the entropy effect (pre-exponential factor) of the reaction. The Arrhenius activation energy of an entropically

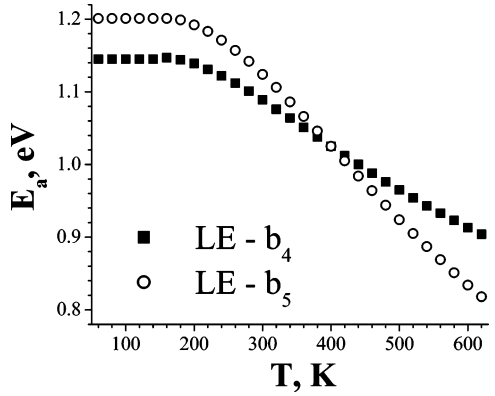

Figure 6. Temperature dependence of Arrhenius activation energies for the formation of $\mathbf{b}_4$ and $\mathbf{b}_5$ ions calculated using Tolman's theorem.

unfavorable reaction 1 decreases faster with increase in temperature than the Arrhenius activation energy of reaction 2 characterized by a more positive entropy effect and a higher pre-exponential factor. The two curves shown in Figure 6 cross at ca. 400 K. At higher temperatures, the activation energy of reaction 1 becomes smaller than the activation energy for reaction 2. Figure 6 clearly demonstrates that assessment of the relative stability of different ions toward dissociation using relative Arrhenius activation energies must be done with great care because the relative values are affected both by the differences in entropy effects for reactions and by the differences between the temperatures used in experiments.

Conclusions

We have performed a detailed analysis of time- and energy-resolved SID data of protonated leucine enkephalin, a well-studied model peptide commonly used as a "thermometer" ion for characterization of internal excitation of gas-phase biomolecules in different ionization and activation methods. SID of this model peptide is well described using seven primary and four secondary fragmentation pathways. The energetics and dynamics of the seven primary dissociation channels were deduced from RRKM-based modeling of time- and energy-resolved fragmentation efficiency curves of the precursor ion and its fragments. We found that the lowest-energy dissociation channels resulting in formation of the $\mathbf{b}_4$ and $\mathbf{b}_5$ ions are associated with very tight transition states while higher-energy pathways are entropically more favorable. These include formation of the $\mathbf{a}_4$, **y** ions, internal fragments, and phenylalanine immonium ion directly from the protonated precursor ion. We suggested that these higher-energy dissociation pathways are strongly suppressed in experiments that utilize slow stepwise ion activation approaches. Reactive fractions calculated by averaging microcanonical rate constants over thermal energy distribution at 450 K showed that in thermal experiments conducted at this temperature only 8% of the $\mathbf{a}_4$ ions are formed from the parent ion and the rest of the population of this fragment ion originates from consecutive fragmentation of the $\mathbf{b}_4$ ion. In contrast, in out SID experiments 100% of the $\mathbf{a}_4$ ions are formed directly from the parent ion. Fast ion activation offered by ion-surface collisions allows us to explore the details of the energetics and mechanisms of peptide fragmentation without introducing ambiguities associated with competition between ion activation and dissociation processes. We have also demonstrated that detailed understanding of the fragmentation behavior following single-step fast ion activation provides a solid platform for understanding fragmentation patterns obtained in slow heating experiments.

Comparison of dissociation parameters for the formation of the $\mathbf{b}_4$ and $\mathbf{b}_5$ ions obtained in this study with Arrhenius activation parameters reported by Williams and co-workers demonstrated for the first time that Arrhenius activation energies do not necessarily follow the same order as the corresponding threshold energies. In particular, our modeling showed that the threshold energy for the formation of the $\mathbf{b}_4$ ion (1.14 eV) is lower than the threshold energy for the formation of the $\mathbf{b}_5$ ion (1.20 eV). In contrast, BIRD data showed an opposite behavior: the activation energy of the $MH^+ \rightarrow \mathbf{b}_4$ channel (1.11 eV) is higher than the activation energy of the $MH^+ \rightarrow \mathbf{b}_5$ channel (0.99 eV). We have previously demonstrated that the Arrhenius activation energy reflects not only the energetics of dissociation but also contains a significant entropic contribution. The difference between the order of activation and threshold energies for these two reactions is a direct consequence of the difference in entropic contributions to the corresponding Arrhenius activation energies. Arrhenius activation energies calculated from the corresponding threshold energies show strong temperature dependence. The decrease in the activation energy with temperature is faster for reactions with lower pre-exponential factors. Conversion of activation energies into threshold energies using Tolman theorem is the only approach for accurate determination of the relative stability of gas-phase ions from thermal experiments.

Acknowledgment. This paper is dedicated to the memory of my mentor, Chava Lifshitz—a great scientist, an excellent teacher, and a good friend. The research described in this manuscript was performed at the W. R. Wiley Environmental Molecular Sciences Laboratory (EMSL), a national scientific user facility sponsored by the U.S. Department of Energy's Office of Biological and Environmental Research and located at Pacific Northwest National Laboratory (PNNL). PNNL is operated by Battelle for the U.S. Department of Energy. Research at EMSL was supported by the grant from the Separations and Analysis Program within the Chemical Sciences Division, Office of Basic Energy Sciences of the U.S. Department of Energy.

References and Notes

(1) Dunbar, R. C. *J. Phys. Chem.* **1994**, *98*, 8705−8712.
(2) Price, W. D.; Schnier, P. D.; Jockusch, R. A.; Strittmatter, E. F.; Williams, E. R. *J. Am. Chem. Soc.* **1996**, *118*, 10640−10644.
(3) Dunbar, R. C.; McMahon, T. B. *Science* **1998**, *279*, 194−197.
(4) Price, W. D.; Schnier, P. D.; Williams, E. R. *J. Phys. Chem. B* **1997**, *101*, 664−673.
(5) Schnier, P. D.; Price, W. D.; Jockusch, R. A.; Williams, E. R. *J. Am. Chem. Soc.* **1996**, *118*, 7178−7189.
(6) Jockusch, R. A.; Schnier, P. D.; Price, W. D.; Strittmatter, E. F.; Demirev, P. A.; Williams, E. R. *Anal. Chem.* **1997**, *69*, 1119−1126.
(7) Tolman, R. C. *J. Am. Chem. Soc.* **1920**, *42*, 2506−2528.
(8) Gilbert, R. G.; Smith, S. C. *Theory of Unimolecular and Recombination Reactions*; Blackwell Scientific Publications: Oxford, UK, 1990.
(9) Dunbar, R. C. *J. Chem. Phys.* **1991**, *95*, 2537−2548.
(10) Baer, T.; Hase, W. L. *Unimolecular Reaction Dynamics: Theory and Experiments*; Oxford University Press: New York, 1996.
(11) Laskin, J.; Futrell, J. H. *J. Phys. Chem. A* **2003**, *107*, 5836−5839.
(12) Laskin, J.; Byrd, M.; Futrell, J. *Int. J. Mass Spectrom.* **2000**, *196*, 285−302.
(13) Laskin, J.; Futrell, J. *J. Phys. Chem. A* **2000**, *104*, 5484−5494.
(14) Alexander, A. J.; Boyd, R. K. *Int. J. Mass Spectrom Ion Processes* **1989**, *90*, 211−240.
(15) Bier, M. E.; Schwartz, J. C.; Schey, K. L.; Cooks, R. G. *Int. J. Mass Spectrom Ion Processes* **1990**, *103*, 1−19.
(16) Ballard, K. D.; Gaskell, S. J. *Int. J. Mass Spectrom Ion Processes* **1991**, *111*, 173−189.
(17) Cole, R. B.; Lemeillour, S.; Tabet, J. C. *Anal. Chem.* **1992**, *64*, 365−371.
(18) McCormack, A. L.; Somogyi, A.; Dongre, A. R.; Wysocki, V. H. *Anal. Chem.* **1993**, *65*, 2859−2872.

(19) Cheng, X. H.; Wu, Z. C.; Fenselau, C.; Ishihara, M.; Musselman, B. D. *J. Am. Soc. Mass Spectrom.* **1995**, *6*, 175−186.

(20) Yalcin, T.; Csizmadia, I. G.; Peterson, M. R.; Harrison, A. G. *J. Am. Soc. Mass Spectrom.* **1996**, *7*, 233−242.

(21) Vachet, R. W.; Bishop, B. M.; Erickson, B. W.; Glish, G. L. *J. Am. Chem. Soc.* **1997**, *119*, 5481−5488.

(22) Vachet, R. W.; Ray, K. L.; Glish, G. L. *J. Am. Soc. Mass Spectrom.* **1998**, *9*, 341−344.

(23) Rakov, V. S.; Borisov, O. V.; Whitehouse, C. M. *J. Am. Soc. Mass Spectrom.* **2004**, *15*, 1794−1809.

(24) Schnier, P. D.; Price, W. D.; Strittmatter, E. F.; Williams, E. R. *J. Am. Soc. Mass Spectrom.* **1997**, *8*, 771−780.

(25) Goeringer, D. E.; Asano, K. G.; McLuckey, S. A. *Int. J. Mass Spectrom.* **1999**, *183*, 275−288.

(26) Asano, K. G.; Goeringer, D. E.; McLuckey, S. A. *Int. J. Mass Spectrom.* **1999**, *187*, 207−219.

(27) Schnier, P. D.; Jurchen, J. C.; Williams, E. R. *J. Phys. Chem. B* **1999**, *103*, 737−745.

(28) Drahos, L.; Heeren, R. M. A.; Collette, C.; De Pauw, E.; Vekey, K. *J. Mass Spectrom.* **1999**, *34*, 1373−1379.

(29) Mabud, M. D. A.; Dekrey, M. J.; Cooks, R. G. *Int. J. Mass Spectrom Ion Processes* **1985**, *67*, 285−294.

(30) Cooks, R. G.; Ast, T.; Pradeep, T.; Wysocki, V. *Acc. Chem. Res.* **1994**, *27*, 316−323.

(31) Dongre, A. R.; Somogyi, A.; Wysocki, V. H. *J. Mass Spectrom.* **1996**, *31*, 339−350.

(32) Grill, V.; Shen, J.; Evans, C.; Cooks, R. G. *Rev. Sci. Instrum.* **2001**, *72*, 3149−3179.

(33) Laskin, J.; Futrell, J. H. *J. Am. Soc. Mass Spectrom.* **2003**, *14*, 1340−1347.

(34) Meroueh, O.; Hase, W. L. *J. Am. Chem. Soc.* **2002**, *124*, 1524−1531.

(35) Laskin, J.; Denisov, E.; Futrell, J. *J. Am. Chem. Soc.* **2000**, *122*, 9703−9714.

(36) Laskin, J. *Eur. J. Mass Spectrom.* **2004**, *10*, 259−267.

(37) Laskin, J.; Denisov, E.; Futrell, J. H. *J. Phys. Chem. B* **2001**, *105*, 1895.

(38) Laskin, J.; Bailey, T. H.; Denisov, E. V.; Futrell, J. H. *J. Phys. Chem. A* **2002**, *106*, 9832−9836.

(39) Laskin, J.; Denisov, E. V.; Shukla, A. K.; Barlow, S. E.; Futrell, J. H. *Anal. Chem.* **2002**, *74*, 3255−3261.

(40) Shaffer, S. A.; Tang, K. Q.; Anderson, G. A.; Prior, D. C.; Udseth, H. R.; Smith, R. D. *Rapid Commun. Mass Spectrom.* **1997**, *11*, 1813−1817.

(41) Senko, M. W.; Canterbury, J. D.; Guan, S. H.; Marshall, A. G. *Rapid Commun. Mass Spectrom.* **1996**, *10*, 1839−1844.

(42) Holbrook, K. A.; Pilling, M. J.; Robertson, S. H. *Unimolecular Reactions*, 2nd ed.; John Wiley & Sons: New York, 1996.

(43) Derrick, P. J.; Loyd, P. M.; Christie, J. R. In *Advances in Mass Spectrometry*; Cornides, I., Howárth, G., Vékey, K., Eds.; Wiley: Chichester, 1995; Vol. 13.

(44) Vestal, M. L. *J. Chem. Phys.* **1965**, *43*, 1356.

(45) Bente, P. F.; McLafferty, F. W.; McAdoo, D. J.; Lifshitz, C. *J. Phys. Chem.* **1975**, *79*, 713−721.

(46) Miller, S. A.; Luo, H.; Pachuta, S. J.; Cooks, R. G. *Science* **1997**, *275*, 1447−1450.

(47) Gologan, B.; Green, J. R.; Alvarez, J.; Laskin, J.; Cooks, R. G. *Phys. Chem. Chem. Phys.* **2005**, *7*, 1490−1500.

(48) Laskin, J.; Bailey, T. H.; Futrell, J. H. *Int. J. Mass Spectrom.* **2006**, *249*, 462−472.

(49) Laskin, J.; Denisov, E.; Futrell, J. H. *Int. J. Mass Spectrom.* **2002**, *219*, 189−201.

(50) It should be noted that, although reaction 4 describes the formation of the $\mathbf{b}_3$, $\mathbf{b}_2$, and Y ions, its energetics and dynamics represent the energetics and dynamics of formation of the $\mathbf{b}_3$ ion because the $\mathbf{b}_2$ and Y ions are products of the primary $\mathbf{b}_3$ fragment.

(51) Paizs, B.; Suhai, S. *J. Am. Soc. Mass Spectrom.* **2004**, *15*, 103−113.

(52) Ustyuzhanin, P.; Kogan, A.; Reuben, B. G.; Lifshitz, C. *Int. J. Chem. Kinet.* **2001**, *33*, 707−714.

(53) Jalkanen, K. J. *J. Phys.: Condens. Matter* **2003**, *15*, S1823−S1851.

(54) McLuckey, S. A.; Goeringer, D. E. *J. Mass Spectrom.* **1997**, *32*, 461−474.

(55) Nemykin, V. N.; Laskin, J.; Basu, P. *J. Am. Chem. Soc.* **2004**, *126*, 8604−8605.

(56) Dongre, A. R.; Jones, J. L.; Somogyi, A.; Wysocki, V. H. *J. Am. Chem. Soc.* **1996**, *118*, 8365−8374.

(57) Jockusch, R. A.; Paech, K.; Williams, E. R. *J. Phys. Chem. A* **2000**, *104*, 3188−3196.